J. Fluid Mech. (2003), *vol.* 485, *pp.* 307–335.
DOI: 10.1017/S0022112003004518 Printed in the United Kingdom

The absorption of axial acoustic waves by a perforated liner with bias flow

By JEFF D. ELDREDGE AND ANN P. DOWLING

Department of Engineering, University of Cambridge, Trumpington Street, Cambridge CB2 1PZ, UK

(Received 23 August 2002 and in revised form 29 January 2003)

The effectiveness of a cylindrical perforated liner with mean bias flow in its absorption of planar acoustic waves in a duct is investigated. The liner converts acoustic energy into flow energy through the excitation of vorticity fluctuations at the rims of the liner apertures. A one-dimensional model that embodies this absorption mechanism is developed. It utilizes a homogeneous liner compliance adapted from the Rayleigh conductivity of a single aperture with mean flow. The model is evaluated by comparing with experimental results, with excellent agreement. We show that such a system can absorb a large fraction of incoming energy, and can prevent all of the energy produced by an upstream source in certain frequency ranges from reflecting back. Moreover, the bandwidth of this strong absorption can be increased by appropriate placement of the liner system in the duct. An analysis of the acoustic energy flux is performed, revealing that local differences in fluctuating stagnation enthalpy, distributed over a finite length of duct, are responsible for absorption, and that both liners in a double-liner system are absorbant. A reduction of the model equations in the limit of long wavelength compared to liner length reveals an important parameter grouping, enabling the optimal design of liner systems.

1. Introduction

Perforated liners are used in engineering systems for their ability to absorb sound. In particular, modern combustion systems such as gas turbines and jet engines are often operated under conditions that make them susceptible to combustion instabilities, and by including a passive damping device, such as a liner, these acoustically driven instabilities can be suppressed. The high temperatures present in the jet flows of these systems require that a bias flow be blown through a perforated liner to protect the walls of the duct enclosing the jet. Remarkably, this bias flow has been found to be capable of providing the additional benefit of improving the effectiveness of the liner as an absorber of sound. In the present work we investigate the effectiveness of a perforated liner with bias flow in absorbing planar acoustic waves propagating in a duct of circular cross-section.

Early work considered the behaviour of perforated liners in the absence of mean flow. The reflection and transmission properties of an infinite plane perforated by a homogeneous array of orifices were examined by Ffowcs Williams (1972). Leppington & Levine (1973) performed the same analysis with the help of an integral equation, which allowed a correction to the Ffowcs Williams result. They also considered the case when the screen is backed by an infinite rigid wall. Acoustic liners are never infinite, however, and the acoustic properties of a semi-infinite perforated screen were

investigated by Leppington (1977) using a Wiener–Hopf approach. In the absence of flow, no damping mechanisms are present in the linear acoustic equations; only the inclusion of nonlinear effects can predict dissipation of sound. For example, Cummings (1983) considered power losses due to high-amplitude sound transmission through orifice plates, which required that nonlinear terms be included in the analysis.

If the holes in a perforated screen are sufficiently separated relative to their diameter, then they nearly behave as though in isolation. Consequently, theoretical investigations of perforated screens can utilize the significant amount of work carried out in exploring the acoustic properties of a single orifice. Howe (1979*b*) developed an expression for the Rayleigh conductivity of an aperture through which a high-Reynolds-number flow passes. In such a configuration, viscous effects are limited to the separation of the flow from the rim of the aperture. The harmonic pressure difference across the orifice thus leads to the periodic shedding of vorticity, and consequently acoustic energy is converted into mechanical energy, which is subsequently dissipated into heat. This mechanism is linear, in the sense that the fraction of incident sound energy that is absorbed is independent of the amplitude of the sound. The phenomenon is also present in flow issuing from a nozzle (Howe 1979*a*), trailing edge flow (Howe 1986*b*) and abrupt area expansions (Dupère & Dowling 2000). In each example, an unsteady Kutta condition is applied to determine the magnitude of the fluctuating vorticity. The applicability of this condition was addressed by Crighton (1985), who discussed its consequences in several contexts, including the input of acoustic energy into the vortical motion of a shear layer.

The vortex shedding mechanism was studied further by Hughes and Dowling, who presented analyses of screens with regular arrays of slits (Dowling & Hughes 1992) and circular perforations (Hughes & Dowling 1990) with mean bias flows, to suppress the screech instability. They showed that if a rigid backing wall is included, it is theoretically possible to absorb all impinging sound at a particular frequency, because reflection from the wall allows substantially more interaction between the sound and screen. The perforated liner arrangement was investigated experimentally by Jing & Sun (1999), with an additional term included in the model to account for screen thickness. Their results revealed that the thickness of the screen is crucial, and in subsequent work (Jing & Sun 2000) they numerically solved the governing equation for a single aperture in a thick plate. Their results reduce to those of Howe (1979*b*) in the limit of zero thickness. These investigations only considered acoustic waves that impinge upon a perforated screen. Many acoustically driven instabilities primarily contain axial acoustic modes, however, and the present investigation focuses on the absorptive properties of a cylindrical perforated liner in the presence of planar duct modes.

Cellular acoustic liners, which consist of regular arrays of cavities, have also been investigated. These liners rely primarily on Helmholtz resonance of the cavities for absorption. Ko (1972) performed an analysis of a circular duct with such a liner, with a uniform mean flow present in the duct, using a finite difference approximation of the equations. While most theoretical investigations have been carried out in the frequency domain, Sbardella, Tester & Imregun (2001) used a time-domain approach to develop a one-dimensional model for the acoustic response of a typical liner cavity, and coupled this model to the solution of the two-dimensional duct flow equations. Tam *et al.* (2001) used direct numerical simulation to explore the dissipation mechanisms of a single liner cavity in detail, and confirmed previous observations that vortex shedding is the dominant mechanism of absorption for incident waves of high amplitude. The

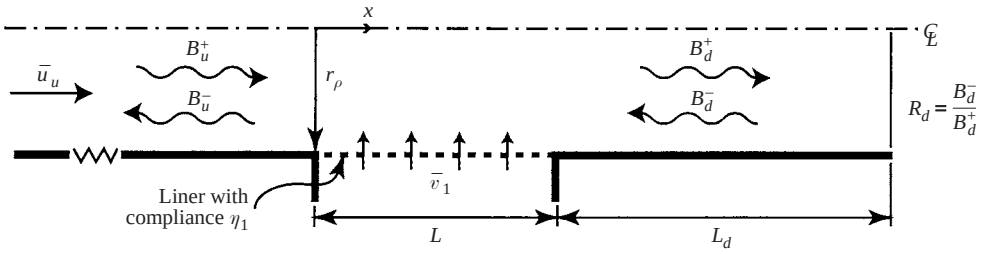

FIGURE 1. Schematic of acoustic waves and flow quantities in a lined duct.

use of bias flow to improve the performance of acoustic liners has recently been investigated by Follet, Belts & Kelly (2001).

The present investigation will consist of both modelling and experiment. Our model will be based on the Rayleigh conductivity of Howe (1979*b*), and like Hughes & Dowling (1990) and Jing & Sun (1999) we will develop an effective liner compliance based on the principle that unsteady vortex shedding from the aperture rims is the primary mechanism for absorption. In § 2 the model equations will be developed, and the treatment of different liner configurations will be discussed. In § 3 the nature of liner absorption will be analysed, which will provide useful insight for designing more effective liners. The model equations will be solved and compared with experimental results in § 4. Finally, in § 5 we will identify important parameters that enable the optimal design of liner systems, which we will discuss at length.

2. Model

A quasi-one-dimensional lined-duct model is developed in this section, beginning with the derivation of a set of equations for the acoustic quantities in a duct with a general wall compliance. The compliance has been defined by Leppington (1977) as the ratio of the normal derivative of a quantity on a surface to its jump across the surface. In the case of the stagnation enthalpy perturbation, which we use here,

$$\frac{\partial B'}{\partial n} = \eta [B']_{0-}^{0+}, \tag{2.1}$$

where n is the wall normal. We will construct an effective compliance for the liner based on the results of Howe (1979*b*) for a single aperture with steady flow.

2.1. *Lined-duct equations*

Consider a circular duct of uniform cross-section, consisting of two sections with rigid walls, separated by a lined section for which the compliance is uniformly equal to η_1 (see figure 1). A steady flow of velocity $\bar{u}_u$ is present in the upstream duct, as well as a steady inward bias flow through the liner of uniform average velocity $\bar{v}_1$. The subscript on $\bar{v}_1$ denotes it, as well as other quantities and parameters, as describing liner 1, the innermost liner. Another liner would be denoted by subscript 2, and so on. Both mean flows are small and the stagnation temperatures associated with them are equal. Thus, the mean density can be uniformly approximated by $\bar{\rho}$ and the mean speed of sound by $\bar{c}$. If the length of the lined section is L, and the cross-sectional area and circumference of the duct are S_p and C_1 respectively, then the downstream flow velocity is $\bar{u}_d = \bar{u}_u + (C_1 L/S_p)\bar{v}_1$. As there are no circumferential variations in the flow or boundary conditions, the problem is axisymmetric.

The axial position is denoted by x, and $x = 0$ coincides with the interface of the lined section and the upstream duct. Harmonic pressure fluctuations are produced in the upstream section, of sufficiently low frequency that only plane waves are allowed to propagate. Because of the mean flow, it is more natural to describe the acoustic waves in terms of fluctuating stagnation enthalpy, $B' = p'/\bar{\rho} + \bar{u}u'$, where p' is the fluctuating pressure and u' is the fluctuating axial velocity. Thus, in the upstream section, these fluctuations have the form

$$B'(x,t) = \hat{B}(x)\exp[\mathrm{i}\omega t] = B_u^+ \exp[\mathrm{i}(\omega t - k_u^+ x)] + B_u^- \exp[\mathrm{i}(\omega t + k_u^- x)], \quad x < 0, \tag{2.2a}$$

where ω is the angular frequency and k_u^+ and k_u^- are the forward- and backward-travelling wavenumbers, respectively. We adopt the usual convention that only the real components of these fluctuations are physically relevant. In the downstream section, the fluctuations are of the same form,

$$B'(x,t) = \hat{B}(x)\exp[\mathrm{i}\omega t] = B_d^+ \exp[\mathrm{i}(\omega t - k_d^+ x)] + B_d^- \exp[\mathrm{i}(\omega t + k_d^- x)], \quad x > L. \tag{2.2b}$$

The two amplitudes in the downstream section, $B_d^{\pm}$, are related by a known boundary condition. A generic relationship will be assumed, $B_d^- = R_d B_d^+$, where R_d is the reflection coefficient. In § 2.3 we will discuss the specific form of R_d.

We introduce the dimensionless variables

$$\left.\begin{array}{llll} x \to x/L, & t \to \bar{c}t/L, & u \to u/\bar{c}, & v \to v/\bar{c}, \\ B \to B/\bar{c}^2, & \rho \to \rho/\bar{\rho}, & p \to p/(\bar{\rho}\bar{c}^2), & \end{array}\right\} \tag{2.3}$$

and define the upstream and downstream Mach numbers, $M_u = \bar{u}_u/\bar{c}$ and $M_d = \bar{u}_d/\bar{c}$, respectively, and the bias flow Mach number, $M_{l,1} = \bar{v}_1/\bar{c}$. The one-dimensional inviscid equations of motion give the wavenumbers as

$$k_u^+ = \frac{k}{1+M_u}, \quad k_u^- = \frac{k}{1-M_u}, \tag{2.4a, b}$$

$$k_d^+ = \frac{k}{1+M_d}, \quad k_d^- = \frac{k}{1-M_d}, \tag{2.4c, d}$$

where $k \equiv \omega/\bar{c}$. The velocity fluctuations in each of these two sections also follow, with amplitudes

$$\hat{u}(x) = \frac{B_u^+}{1+M_u}\exp(-\mathrm{i}k_u^+ Lx) - \frac{B_u^-}{1-M_u}\exp(\mathrm{i}k_u^- Lx), \quad x < 0, \tag{2.5a}$$

$$\hat{u}(x) = \frac{B_d^+}{1+M_d}\exp(-\mathrm{i}k_d^+ Lx) - \frac{B_d^-}{1-M_d}\exp(\mathrm{i}k_d^- Lx), \quad x > 1. \tag{2.5b}$$

In the lined region $0 < x < 1$, the stagnation enthalpy and velocity have the form

$$B(x,t) = \bar{B} + \hat{B}(x)\,\mathrm{e}^{\mathrm{i}kLt}, \tag{2.6a}$$

$$u(x,t) = \bar{u}(x) + \hat{u}(x)\,\mathrm{e}^{\mathrm{i}kLt}. \tag{2.6b}$$

Note that the mean axial velocity varies with x. To first order,

$$\bar{u}(x) = M_u + \frac{C_1 L}{S_p} M_{l,1} x. \tag{2.7}$$

To connect the three sections, we require that the stagnation enthalpy and velocity perturbations match at $x = 0$ and $x = 1$:

$$\hat{B}(0) = B_u^+ + B_u^-, \tag{2.8a}$$

$$\hat{u}(0) = \frac{B_u^+}{1 + M_u} - \frac{B_u^-}{1 - M_u}, \tag{2.8b}$$

$$\hat{B}(1) = B_d^+(\exp(-\mathrm{i}k_d^+ L) + R_d \exp(\mathrm{i}k_d^- L)), \tag{2.8c}$$

$$\hat{u}(1) = B_d^+ \left(\frac{\exp(-\mathrm{i}k_d^+ L)}{1 + M_d} - \frac{R_d \exp(\mathrm{i}k_d^- L)}{1 - M_d} \right). \tag{2.8d}$$

We will develop equations in $x \in [0, 1]$ for $\hat{B}(x)$ and $\hat{u}(x)$ by appealing to a balance of mass and momentum with respect to a control volume at x that spans the duct cross-section and has infinitesimal axial length, $\mathrm{d}x$. First we define a continuous flow distribution through the liner, $v_1(x, t)$, positive for inward flow. As with other quantities, v_1 is the sum of a mean part and harmonic perturbation,

$$v_1(x, t) = \bar{v}_1 + \hat{v}_1(x)\, \mathrm{e}^{\mathrm{i}kLt}. \tag{2.9}$$

A balance of mass across the control volume leads to

$$\frac{\partial \rho}{\partial t} + \frac{\partial}{\partial x}(\rho u) = \frac{C_1 L}{S_p} \rho v_1. \tag{2.10}$$

The flow through the liner acts like a source (or sink) of mass. From momentum balance we obtain

$$\rho \frac{\partial u}{\partial t} + \rho u \frac{\partial u}{\partial x} + \frac{\partial p}{\partial x} = 0, \tag{2.11}$$

which is simply the one-dimensional Euler equation.

By introducing the mean-harmonic forms of the quantities, and matching terms with linear dependence on fluctuating components, we can form acoustic perturbations of equations (2.10) and (2.11). We also assume that the fluctuations are isentropic, so $\rho' = B' - \bar{u}u'$. We arrive at

$$\mathrm{i}kL\hat{B} + 2\bar{u}\frac{\mathrm{d}\hat{B}}{\mathrm{d}x} + (1 - \bar{u}^2)\frac{\mathrm{d}\hat{u}}{\mathrm{d}x} = \frac{C_1 L}{S_p}\hat{v}_1, \tag{2.12a}$$

$$\mathrm{i}kL\hat{u} + \frac{\mathrm{d}\hat{B}}{\mathrm{d}x} = 0. \tag{2.12b}$$

The equations are more amenable to solution if we express them in terms of the new characteristic quantities,

$$\psi^+ \equiv \tfrac{1}{2}(1 + \bar{u})[\hat{B} + (1 - \bar{u})\hat{u}], \tag{2.13a}$$

$$\psi^- \equiv \tfrac{1}{2}(1 - \bar{u})[\hat{B} - (1 + \bar{u})\hat{u}]. \tag{2.13b}$$

In an unlined duct, plane waves obey the relation $u' = \pm B'/(1 \pm M)$ and the quantities revert to $(\psi^+, \psi^-) = (\hat{B}, 0)$ for forward-travelling waves or $(\psi^+, \psi^-) = (0, \hat{B})$ for backward-travelling waves. When these quantities are substituted into equations (2.12*a*) and (2.12*b*), we arrive at

$$\frac{\mathrm{d}\psi^+}{\mathrm{d}x} = -\frac{\mathrm{i}kL}{1 + \bar{u}}\psi^+ + \frac{1}{2}\frac{C_1 L}{S_p}\hat{v}_1, \tag{2.14a}$$

$$\frac{\mathrm{d}\psi^-}{\mathrm{d}x} = \frac{\mathrm{i}kL}{1-\bar{u}}\psi^- - \frac{1}{2}\frac{C_1 L}{S_p}\hat{v}_1. \tag{2.14b}$$

Through equations (2.8*a–d*), the boundary values of ψ^+ and ψ^- are

$$\psi^+(0) = B_u^+, \quad \psi^+(1) = B_d^+ \exp(-\mathrm{i}k_d^+ L), \tag{2.15a, b}$$

$$\psi^-(0) = B_u^-, \quad \psi^-(1) = B_d^- \exp(\mathrm{i}k_d^- L). \tag{2.15c, d}$$

Since the equations are first order, we need only enforce two boundary conditions. It is sufficient to assume that the amplitude, B_u^+, of the incident wave is known, relative to which all other amplitudes are measured. The downstream reflection depends only on geometry and mean flow conditions, and can be used to define a linear relationship between fluctuating quantities. We thus enforce

$$\psi^+(0) = B_u^+, \tag{2.16a}$$

$$\psi^-(1)\exp(-\mathrm{i}k_d^- L) - \psi^+(1) R_d \exp(\mathrm{i}k_d^+ L) = 0. \tag{2.16b}$$

Equations (2.14*a*, *b*) are not closed, however, and the fluctuating liner flow, $\hat{v}_1$ must be considered. The assumed compliance of the liner, η_1, implies a local relationship between $\hat{v}_1$ and the difference in stagnation enthalpy fluctuations across the liner. Using (2.1) in conjunction with the linearized momentum equation in the normal direction and the relation $\hat{B} = \psi^+ + \psi^-$, we arrive at

$$\hat{v}_1(x) = \frac{\eta_1}{\mathrm{i}kL}[\hat{B}_1(x) - \psi^+(x) - \psi^-(x)], \tag{2.17}$$

where $\hat{B}_1$ is the fluctuating part of the stagnation enthalpy external to the liner, $B_1(x,t) = \bar{B}_1 + \hat{B}_1(x)\exp(\mathrm{i}kLt)$. The behaviour of $\hat{B}_1$ depends upon the specific configuration of the duct system. We consider three:

Configuration 1. Open exterior. When the liner is exposed to the ambient environment it is satisfactory to assume that the pressure fluctuations (and hence stagnation enthalpy fluctuations, since the two quantities are proportionally related in the absence of mean flow) on the outside of the liner are zero. Thus, in this configuration,

$$\hat{v}_1(x) = -\frac{\eta_1}{\mathrm{i}kL}\hat{B}(x) = -\frac{\eta_1}{\mathrm{i}kL}[\psi^+(x) + \psi^-(x)], \tag{2.18}$$

and the system (2.14*a*, *b*) and (2.18) is closed. Note that for this relation to be appropriate, the exterior of the liner need only be exposed to a region in which pressure fluctuations are negligibly small. Thus, a large enclosing cavity of volume $V \gg C_1 L/k$ is ensured to behave sufficiently similarly to a plenum to justify the assumption.

Configuration 2. Annular cavity enclosed by rigid wall. In this configuration the liner is surrounded by an annular cavity formed by a larger rigid cylinder. The cavity is of the same axial length as the liner, with rigid walls at each end. If the cavity is sufficiently shallow, then the acoustic equations in this region are one-dimensional, as in the duct. Using a similar balance of mass and momentum through an annular control volume of length $\mathrm{d}x$ leads to the non-dimensional equations

$$\frac{\mathrm{d}\hat{B}_1}{\mathrm{d}x} = -\mathrm{i}kL\hat{u}_1, \tag{2.19a}$$

$$\frac{\mathrm{d}\hat{u}_1}{\mathrm{d}x} = -\mathrm{i}kL\hat{B}_1 - \frac{C_1 L}{S_c}\hat{v}_1, \tag{2.19b}$$

where S_c is the cross-sectional area of the annular cavity. Together with the rigid-wall boundary conditions

$$\hat{u}_1(0) = 0, \quad \hat{u}_1(1) = 0, \tag{2.20}$$

equations (2.14*a*, *b*), (2.17) and (2.19*a*, *b*) now form a closed system of four differential equations for the four unknowns ψ^+, ψ^-, $\hat{B}_1$ and $\hat{u}_1$. Note that such a configuration is not practically feasible if a bias flow is present, as there must be an inlet in the cavity for the mass flow. However, if this inlet is choked, then the rigid-wall approximation is likely to be sufficient.

Configuration 3. Annular cavity enclosed by second liner. This configuration is very similar to the previous one, except that the annular cavity is now formed by a second perforated liner. This arrangement might be found in a cooling flow system, in which the outer skin supplies jets that impinge upon the outer surface of the inner liner. We will assign compliance η_2 and circumference C_2 to the outer cylinder. Then the equations in the cavity are

$$\frac{\mathrm{d}\hat{B}_1}{\mathrm{d}x} = -\mathrm{i}kL\hat{u}_1, \tag{2.21a}$$

$$\frac{\mathrm{d}\hat{u}_1}{\mathrm{d}x} = -\mathrm{i}kL\hat{B}_1 - \frac{C_1 L}{S_c}\hat{v}_1 + \frac{C_2 L}{S_c}\hat{v}_2, \tag{2.21b}$$

where $\hat{v}_2$ is the inward fluctuating flow through the outer liner, related to the stagnation enthalpy difference across the liner by

$$\hat{v}_2(x) = \frac{\eta_2}{\mathrm{i}kL}[\hat{B}_2(x) - \hat{B}_1(x)]. \tag{2.22}$$

The boundary conditions for the cavity quantities are the same as before, (2.20). The system of equations (2.14*a*, *b*), (2.17) and (2.20)–(2.22) is closed with some treatment of $\hat{B}_2$, the fluctuating stagnation enthalpy external to the second liner, involving one of the three configurations discussed. Note that, through conservation of mass, the mean bias flows through each liner are related,

$$M_{h,1} = \frac{C_2}{C_1}\frac{\sigma_2}{\sigma_1}M_{h,2}. \tag{2.23}$$

It is important to note that this one-dimensional model is only valid when the planar mode is the only propagating mode in the duct. For a circular duct, this limits the maximum frequency to

$$kL < 1.841\left(\frac{1}{2}\frac{C_1 L}{S_p}\right), \tag{2.24}$$

to avoid the cut-on of the lowest azimuthal mode. Regardless of the configuration of the duct–liner system, the system of equations constitutes a boundary value problem. In principle, an analytical solution for this linear system is possible, though with a linearly increasing mean duct flow it requires some effort. Even if the variability of the mean duct flow is neglected, the solution is too complicated to be revealing (though we do present the solution for a liner in Configuration 1 with no mean duct flow in the Appendix). Thus, we solve the system numerically, using a shooting method to enforce boundary conditions at either end of the lined section (see, e.g., Press *et al.* 1986). Before solution is possible, however, an expression for the liner compliance must be developed.

2.2. *Liner compliance*

The acoustic behaviour of a single aperture can be used to develop an expression for the compliance of a homogeneous screen of such apertures, provided that the distance, d, between neighbouring apertures is large compared with their diameters, $2a$, and the acoustic wavelength, λ, is much larger than the inter-aperture distance. Thus, we require $ka \ll kd \ll 1$. This approach has been used by Hughes & Dowling (1990), who adapted the Rayleigh conductivity of a single aperture in a plane proposed by Howe (1979*b*) to construct a smooth compliance for a perforated screen with bias flow. We will use the same approach in the present model.

The Rayleigh conductivity relates the fluctuating aperture volume flux, $Q' = \hat{Q}\exp(\mathrm{i}kLt)$, to the fluctuating difference in stagnation enthalpy across the aperture. In dimensionless form,

$$K = -\mathrm{i}kL\frac{\hat{Q}}{[\hat{B}]_{0^-}^{0^+}}. \tag{2.25}$$

For simplicity, we assume that the screen is composed of a square grid of apertures, with equal distance d between adjacent apertures. The number of apertures per unit area in the screen is $N = 1/d^2$ and the fluctuating liner velocity is equal to $\hat{v} = N\hat{Q}$. Comparing (2.25) with (2.1), with consideration of the linearized momentum equation, the compliance has a simple relationship with the conductivity of a single component aperture,

$$\eta = NL^2K = KL^2/d^2. \tag{2.26}$$

The expression for the conductivity of a single aperture in an infinitely thin wall, derived by Howe (1979*b*), is here adapted to the convention of positive exponent in the harmonic factor $\exp(\mathrm{i}kLt)$,

$$K_a = \frac{2a}{L}(\gamma + \mathrm{i}\delta), \tag{2.27}$$

where a is the radius of the aperture, and γ and δ are given by equations (3.14) of Howe (1979*b*). Each is dependent on only the Strouhal number of the flow, $St = \omega a/U_c$, where U_c is the convection velocity of vortices shed from the aperture rim. Howe argues that this velocity is approximately equal to the mean velocity in the aperture. If σ is the open-area ratio of the perforated screen, $\sigma \equiv \pi a^2/d^2$, then the aperture Mach number, $M_h \approx U_c/\bar{c}$, is related to the mean liner flow through $M_h = M_l/\sigma$, and

$$St \approx \frac{ka}{M_h} = \frac{ka\sigma}{M_l}. \tag{2.28}$$

Howe's model is based on a flow that behaves ideally, except insofar as viscosity is responsible for the creation of vorticity at the sharp rim of the aperture. It neglects many real flow features, such as wall thickness and accompanying boundary layer dissipation. The inertial effect of liner thickness can be approximately accounted for by regarding the stagnation enthalpy difference across the liner as a sum of the contributions to unsteady vortex shedding and acceleration of the fluid in the aperture. This leads to the following expression for the total compliance:

$$\frac{1}{\eta_{tot}} = \frac{\pi a^2}{\sigma L^2}\frac{1}{K_a} + \frac{t}{\sigma L}, \tag{2.29}$$

where t is the liner thickness, which may include a correction for end effects. Jing & Sun (1999) have used this approach in their model, and their comparison with experimental results is favourable. However, their more recent work (Jing & Sun 2000) has demonstrated that the effective thickness decreases with increasing bias flow, behaviour which is absent from (2.29). Bellucci, Paschereit & Flohr (2002) have developed a model for the acoustic impedance of a perforated screen backed by a rigid wall that incorporates several effects, including viscous losses in the aperture and an allowance for reactance of the external flow. Their model agrees well with their experimental results, though they slightly overpredict the magnitude of reflection in a thick screen at resonance. Because our goal is to predict the absorptive properties of a perforated liner, embodied in the imaginary part of the compliance, the thickness is less important than δ to model accurately and expression (2.29) is used. It will be demonstrated that this approach is adequate.

It is worth noting that the Rayleigh conductivity of Howe (1979*b*) is strictly valid in the presence of a mean bias flow only, and not with an additional grazing flow. In subsequent work, Howe, Scott & Sipcic (1996) have numerically computed the Rayleigh conductivity of an aperture with mean grazing flow only. We hypothesize that the bias flow creates a thin boundary layer adjacent to the liner, in which the bias flow is dominant. Vorticity fluctuations at the aperture rim are assumed to convect normally from the liner, and cannot interact with the downstream aperture rim and generate sound as is possible in the analysis of Howe *et al.* (1996). The convected vorticity may eventually reach the edge of the boundary layer and interact with the mean duct flow, but will probably lose coherence in the process and have negligible effect on apertures downstream.

2.3. *Downstream reflection coefficient*

In boundary condition (2.16*b*), the reflection coefficient, R_d, appears and we now discuss its form. In the trivial case of a semi-infinite downstream section, no acoustic waves are reflected and $R_d = 0$. For an unflanged open end, which is more likely to be encountered in practice, previous investigations can be relied upon to develop an appropriate expression. In the absence of a mean duct flow, the reflection is nearly perfect save the small energy lost to radiation. Levine & Schwinger (1948) have solved this problem using a Wiener–Hopf approach. For low frequencies, the specific acoustic impedance of the open end is well approximated by

$$\zeta(kR_p) = \tfrac{1}{4}(kR_p)^2 + \mathrm{i}0.6kR_p, \tag{2.30}$$

where R_p is the radius of the duct. The reflection coefficient is related to ζ by

$$R_d = \frac{\zeta(kR_p) - 1}{\zeta(kR_p) + 1} \exp[-\mathrm{i}2k(L + L_d)], \tag{2.31}$$

where L_d/L is the scaled downstream duct length. Thus, R_d can be approximated to second order in kR_p by

$$R_d = -\left(1 - \tfrac{1}{2}(kR_p)^2\right) \exp[-\mathrm{i}2k(L + L_d + \delta)], \tag{2.32}$$

where $\delta \approx 0.6R_p$ is the end correction.

When mean flow is present, acoustic energy will be removed from the duct through radiation as well as through excitation of jet instability waves (Cargill 1982*a*, *b*; Munt 1977, 1990). The latter effect can be accounted for by imposing a Kutta condition at the edge. Cargill (1982*a*) has solved the problem using the Wiener–Hopf technique

and assumed $kR_p \ll 1$ to arrive at the following formula for R_d, second-order-accurate in kR_p:

$$R_d = -\left|\frac{(1-M^2)g-(1-M)}{(1-M^2)g+(1+M)}\right| \left(1-\tfrac{1}{2}(kR_p)^2\right) \exp[-\mathrm{i}2k((L+L_d)/(1-M^2)+\delta)]. \tag{2.33}$$

The function $g = (g_1 + \mathrm{i}g_2)/M$ is related to the jet instability and is given by Cargill (1982*a*); g_1 and g_2 depend only on the duct Strouhal number, $St_{R_p} = kR_p/M$. For low M and large St_{R_p}, Rienstra (1983) found that the end correction is approximately the same as in the no-flow case. Note that equation (2.33) has been adjusted to represent the reflection of stagnation enthalpy, rather than pressure. For low M, it can be approximated by

$$R_d = -\left(1-\frac{2g_1}{g_1^2+g_2^2}M\right)\left(1-\tfrac{1}{2}(kR_p)^2\right)\exp[-\mathrm{i}2k(L+L_d+\delta)]. \tag{2.34}$$

The magnitude of this formula is in excellent agreement with the results obtained by Munt (1977) numerically.

Peters *et al.* (1993) have demonstrated that (2.34) agrees well with experimental results for $St_{R_p} < 1$. For $St_{R_p} \gtrsim 2$ (as in most cases considered experimentally in the present paper), the coefficient of M in (2.34) tends to 1.1, though the experimental results are less supportive of the formula in this range of Strouhal number. For all cases under our consideration, however, the downstream duct Mach number will be quite small, $M_d \ll 1$, and therefore the precise dependence of the reflection coefficient on the flow is not crucial. Under such a condition, the absorption results from equations (2.32) and (2.34) are indistinguishable.

3. Acoustic energy considerations

To learn more about the nature of the liner absorption, it is useful to analyse the flux of energy in the lined section. The acoustic energy flux vector in a moving flow is given by (Morfey 1971)

$$I_i = \langle B'(\rho u_i)'\rangle = \tfrac{1}{4}[B'(\rho u_i)'^* + B'^*(\rho u_i)'], \tag{3.1}$$

where the angle brackets denote a time average of the product of the real components of these quantities, the superscript $*$ signifies the complex conjugate, and the subscript i denotes the direction ($i = 1$ corresponds to the axial direction, x). We now derive an expression for the rate of change of I_1 with x. First, note that our definition of the quantities ψ^+ and ψ^- provides for a simple relation with the term in brackets in (3.1),

$$I_1 = \tfrac{1}{2}(|\psi^+|^2 - |\psi^-|^2). \tag{3.2}$$

This relation attaches physical significance to ψ^+ and ψ^-. They represent the forward- and backward-transmitted sound intensities in a duct with general wall impedance. The derivative of this relation, when combined with equations (2.14*a*, *b*), leads to

$$\frac{\mathrm{d}I_1}{\mathrm{d}x} = \frac{1}{4}\frac{C_1 L}{S_p}(\psi^+\hat{v}_1^* + \psi^{+*}\hat{v}_1 + \psi^-\hat{v}_1^* + \psi^{-*}\hat{v}_1). \tag{3.3}$$

The first two terms in this expression represent the rate of change of the forward-travelling energy, and the latter two terms correspond to the the backward-travelling

energy change. The liner flow $\hat{v}_1$, through the compliance relation (2.17), couples these rates of change, ensuring that forward-travelling energy is continuously partitioned into a transmitted portion, a portion that is absorbed by the liner and a portion that is reflected upstream, and similarly for the backward-travelling energy.

The quantities ψ^+ and ψ^- are replaced by their definitions (2.13*a*, *b*) to express relation (3.3) in terms of the primitive quantities. We arrive at

$$\frac{\mathrm{d}I_1}{\mathrm{d}x} = \frac{C_1 L}{S_p}\langle B' v_1' \rangle. \tag{3.4}$$

When we integrate this expression over the length of the liner and multiply by the duct area S_p, we arrive at the expected energy balance,

$$S_p[I_1(1) - I_1(0)] = C_1 L \int_0^1 \langle B'(x) v_1'(x) \rangle \, \mathrm{d}x, \tag{3.5}$$

which accounts for the net change in duct energy by the flux of energy through the liner. Because v_1' has been defined as positive for inward flow, when the right-hand side of equation (3.5) is negative, then energy has been absorbed by the liner. Using relation (3.2) with the boundary values of ψ^+ and ψ^-, then

$$\tfrac{1}{2} S_p(|B_d^+|^2 + |B_u^-|^2 - |B_u^+|^2 - |B_d^-|^2) = C_1 L \int_0^1 \langle B'(x) v_1'(x) \rangle \, \mathrm{d}x. \tag{3.6}$$

The acoustic absorption of the liner, Δ, is defined as the net energy absorbed by the liner, scaled by the energy incident upon the lined section. This latter energy is

$$I_{1,in} \equiv \tfrac{1}{2} S_p(|B_u^+|^2 + |B_d^-|^2), \tag{3.7}$$

and thus

$$\Delta \equiv 1 - \frac{|B_d^+|^2 + |B_u^-|^2}{|B_u^+|^2 + |B_d^-|^2} = -\frac{2C_1 L}{S_p} \frac{\displaystyle\int_0^1 \langle B'(x) v_1'(x) \rangle \, \mathrm{d}x}{|B_u^+|^2 + |B_d^-|^2}. \tag{3.8}$$

We now look more closely at the right-hand side of (3.5) to learn more about the nature of the liner absorption. We will assume a configuration of two perforated liners, with compliances η_1 and η_2, respectively, the second liner being exposed to the ambient environment. If we use the compliance relation (2.17), then this leads to

$$\int_0^1 \langle B'(x) v_1'(x) \rangle \, \mathrm{d}x = \int_0^1 \langle B_1'(x) v_1'(x) \rangle \, \mathrm{d}x + \frac{kL}{2} \mathrm{Im}\left(\frac{1}{\eta_1}\right) \int_0^1 |\hat{v}_1(x)|^2 \, \mathrm{d}x. \tag{3.9}$$

An analysis in the annular cavity, similar to the analysis in the duct that led to (3.5), produces on application of the boundary conditions $u_1'(0) = u_1'(1) = 0$,

$$\int_0^1 \langle B_1'(x) v_1'(x) \rangle \, \mathrm{d}x = \frac{C_2}{C_1} \int_0^1 \langle B_1'(x) v_2'(x) \rangle \, \mathrm{d}x. \tag{3.10}$$

Finally, we use the second compliance relation (2.22) with $\hat{B}_2 = 0$, to arrive at

$$\int_0^1 \langle B'(x) v_1'(x) \rangle \, \mathrm{d}x = \frac{kL}{2} \mathrm{Im}\left(\frac{1}{\eta_1}\right) \int_0^1 |\hat{v}_1(x)|^2 \, \mathrm{d}x + \frac{kL}{2} \frac{C_2}{C_1} \mathrm{Im}\left(\frac{1}{\eta_2}\right) \int_0^1 |\hat{v}_2(x)|^2 \, \mathrm{d}x. \tag{3.11}$$

It is apparent from equation (3.11) that, provided that the imaginary part of the compliance of each liner is negative, then there will be a net outward flux of energy through

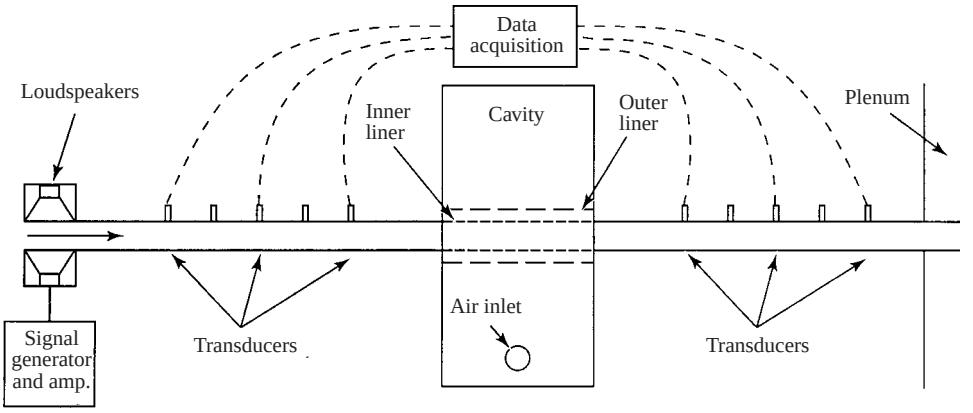

FIGURE 2. Configuration of the perforated liner experiment.

the liner, and acoustic energy in the duct will be absorbed. From equation (2.29) we have

$$\mathrm{Im}\left(\frac{1}{\eta}\right) = -\frac{\pi}{2}\frac{a}{\sigma L}\frac{\delta}{\gamma^2+\delta^2}. \tag{3.12}$$

Because δ is positive for all Strouhal numbers when the Rayleigh conductivity of Howe (1979*b*) is used, the expression is always negative and thus energy is always absorbed. The amount of energy absorbed will depend upon the magnitudes of both terms in (3.11), prediction of which is left to the numerical solution of the model equations.

It is worth contrasting the present model with that of Hughes & Dowling (1990). In their work, an expression for the reflection coefficient of impinging acoustic waves is developed. The absorption mechanism is the same as that considered here, and the same Rayleigh conductivity is used to develop an effective screen compliance. However, their reflection is also dependent upon a so-called 'resonance parameter', $Q \equiv (kd\cos\theta)^2 l/2a$, where l is the distance between the screen and backing wall and θ is the angle of incidence of acoustic waves (i.e. for normally incident sound, $\theta = 0$). The imaginary volume behind each aperture behaves like an individual Helmholtz resonator, and Q measures the proximity of a liner to resonance of this volume. By this theory, $Q = 0$ for waves that travel parallel to the liner, and consequently no absorption is predicted. The crucial difference between this and the present theory is our use of relation (2.17) as a local relationship in x. Rather than depending on a Helmholtz-type resonance for maximum absorption, the integrated effect of local fluctuating stagnation enthalpy difference is responsible.

4. Experiment

4.1. *Experimental set-up*

The experimental apparatus is shown in figure 2. Two equal-length sections of rigid-walled pipe of diameter 12.7 cm and length 80 cm were separated by a section of equal diameter and length 17.8 cm, perforated by a regular lattice of holes of diameter 0.75 mm and spacing 3.3 mm (i.e. $\sigma_1 = 0.040$). This perforated section was surrounded by a duct of diameter 15.2 cm and equal length, perforated by a different array of holes of diameter 2.7 mm and spacing 17.0 mm ($\sigma_2 = 0.020$). The thickness of both perforated liners was 3 mm. The lined section was encased in a large cavity, into which

was fed a steady supply of air by a centrifugal pump to produce bias flow through the liner (measured by a Pitot probe in the cavity inlet), up to a maximum rate of 0.04 $m^3\ s^{-1}$. One end of the duct system had four loudspeakers uniformly arranged about the pipe circumference; the other emptied into a large plenum that allowed air to be drawn through the system independently of the air fed through the lined section. The rate at which this air was drawn (measured by a Pitot probe in the upstream duct section) was limited by flow noise to 0.45 $m^3\ s^{-1}$. The centrelines of the holes in the inner liner were tilted downstream by approximately 45° so that flow passing through them would travel downstream in the duct, even in the absence of a mean duct flow; for this reason the effective thickness of this liner was larger by a factor of $\sqrt{2}$.

Harmonic acoustic waves of magnitude between 90 and 120 dB, and frequency between 100 and 700 Hz, were produced in the duct. This range is well below the cut-on frequency of the first radial mode at 3290 Hz. Three Kulite transducers were arranged on both the upstream and downstream sections to record the pressure fluctuations. From these measurements the amplitudes of the left- and right-travelling acoustic waves in each section were calculated using a two-microphone technique (Seybert & Ross 1977), and thus the fraction of energy entering the lined section that was absorbed could be deduced. The two-microphone formula for the amplitudes P^+ and P^- of these travelling waves in a given section is

$$P^+ = \frac{p_1' \exp[-\mathrm{i}kx_1/(1-M)] - p_2' \exp[-\mathrm{i}kx_2/(1-M)]}{\exp[-\mathrm{i}2kx_1/(1-M^2)] - \exp[-\mathrm{i}2kx_2/(1-M^2)]}, \tag{4.1a}$$

$$P^- = \frac{p_1' \exp[\mathrm{i}kx_1/(1+M)] - p_2' \exp[\mathrm{i}kx_2/(1+M)]}{\exp[\mathrm{i}2kx_1/(1-M^2)] - \exp[\mathrm{i}2kx_2/(1-M^2)]}, \tag{4.1b}$$

where p_1' and p_2' are the measured pressures at transducer positions x_1 and x_2, respectively. With three transducers in each section, three separate pairs could be used to obtain the same amplitudes and thus improve the accuracy. After calculating these amplitudes from both the upstream and downstream sections, equation (3.8) was used to compute the absorption, using the relationship between the pressure and stagnation enthalpy in axial plane waves, $B' = p'(1 \pm M)$, with the positive sign chosen for waves travelling in the mean flow direction and the negative sign for those travelling against it.

The frequency and flow conditions were held constant for each experiment. The transducer signals were low-pass filtered, with the filter cut-off set at 1 kHz. The signals were sampled at a rate of 5 kHz. For the data analysis, 30 contiguous time segments of 1024 samples were recorded. All transducers were calibrated for gain and phase relative to a reference channel, and the reference channel was calibrated absolutely using a pistonphone. The signal coherence between reference and response channels at the frequency of interest was always larger than 0.95. Though the flow-induced noise in the apparatus was significant in some cases, the sound pressure level produced by the loudspeakers was sufficiently high to ensure a strong peak signal for all transducers not situated at pressure nodes.

The three transducers in each section were separated by 20 cm for all experiments below 600 Hz, and by 10 cm for 600 Hz and above. Seybert & Soenarko (1981) have shown that the two-microphone formula is prone to error as the separation of two transducers approaches half a wavelength. Thus, no pair of transducers was used in the formula that was separated by more than 70% of half a wavelength. Furthermore,

the outer transducers were always at least 20 cm from the ends of the duct, by which distance the first higher-order mode would have decayed by 100 dB at 1000 Hz.

For a given set of experiments at several frequencies or flow conditions, the output of the loudspeakers was adjusted so that the sound pressure level at the midpoint of the upstream duct was constant.

4.2. *Results*

For comparison with experimental results, the model equations were solved for each set of flow conditions over the frequency range 0–700 Hz. Configuration 3 was used to close the equations, with the fluctuations external to the outer liner assumed negligible, $B_2' \approx 0$. The latter assumption is justified because the enclosure that encased the liner system was sufficiently large to provide very little stiffness to the fluctuating flow in the outer liner, particularly with the unchoked air inlet, which allowed communication with the environment. For convenience, we summarize the equations here:

$$\frac{\mathrm{d}\psi^+}{\mathrm{d}x} = -\left[\frac{\mathrm{i}kL}{1+\bar{u}(x)} + \frac{1}{2}\frac{C_1 L}{S_p}\frac{\eta_1}{\mathrm{i}kL}\right]\psi^+ - \frac{1}{2}\frac{C_1 L}{S_p}\frac{\eta_1}{\mathrm{i}kL}(\psi^- - \hat{B}_1), \tag{4.2a}$$

$$\frac{\mathrm{d}\psi^-}{\mathrm{d}x} = \left[\frac{\mathrm{i}kL}{1+\bar{u}(x)} + \frac{1}{2}\frac{C_1 L}{S_p}\frac{\eta_1}{\mathrm{i}kL}\right]\psi^- + \frac{1}{2}\frac{C_1 L}{S_p}\frac{\eta_1}{\mathrm{i}kL}(\psi^+ - \hat{B}_1), \tag{4.2b}$$

$$\frac{\mathrm{d}\hat{B}_1}{\mathrm{d}x} = -\mathrm{i}kL\hat{u}_1, \tag{4.2c}$$

$$\frac{\mathrm{d}\hat{u}_1}{\mathrm{d}x} = -\left[\mathrm{i}kL + \frac{C_1 L}{S_c}\frac{\eta_1}{\mathrm{i}kL} + \frac{C_2 L}{S_c}\frac{\eta_2}{\mathrm{i}kL}\right]\hat{B}_1 + \frac{C_1 L}{S_c}\frac{\eta_1}{\mathrm{i}kL}(\psi^+ + \psi^-), \tag{4.2d}$$

$$\psi^+(0) = 1, \quad \psi^-(1)\exp(-\mathrm{i}k_d^- L) - \psi^+(1)R_d\exp(\mathrm{i}k_d^+ L) = 0, \tag{4.2e, f}$$

$$\hat{u}_1(0) = 0, \quad \hat{u}_1(1) = 0, \tag{4.2g, h}$$

where $\bar{u}(x) = M_u + (C_1 L/S_p)M_{l,1}x$ and we have set the amplitude of the incident wave, B_u^+, equal to unity. The compliance for each liner is given by (2.29), and the downstream reflection coefficient by (2.34). These equations are solved for $x \in [0, 1]$ using the shooting method. Once the solution is obtained within the desired tolerance, the absorption is calculated using equation (3.8), which can also be written in terms of ψ^+ and ψ^- as

$$\Delta = \frac{1 + (|R_d|^2 - 1)|\psi^+(1)|^2 - |\psi^-(0)|^2}{1 + |R_d|^2|\psi^+(1)|^2}. \tag{4.3}$$

Before reporting absorption results, we check that our assumed downstream boundary condition compares favourably with the experimental results. Figure 3 compares with theory the real and imaginary parts of the reflection coefficient observed from experiments carried out with a liner bias flow of $M_{h,1} = 0.023$ and no mean duct flow. The agreement is good, with only slight discrepancy at extrema and at 700 Hz. Figure 4 demonstrates the results with a small mean duct flow, $M_u = 0.046$, and liner flow, $M_{h,1} = 0.030$. Once again, the agreement is very good, with a similar discrepancy at 700 Hz.

In the first set of absorption experiments in figure 5, the mean liner bias flow is set at $M_{h,1} = 0.023$ with no mean duct flow. The results from experiments at sound pressure levels of 100 dB and 115 dB are compared with results from solution of the model equations. The absorption undergoes large oscillations between peaks and troughs across the entire range of frequencies, reaching 82% at the peaks, but dropping to

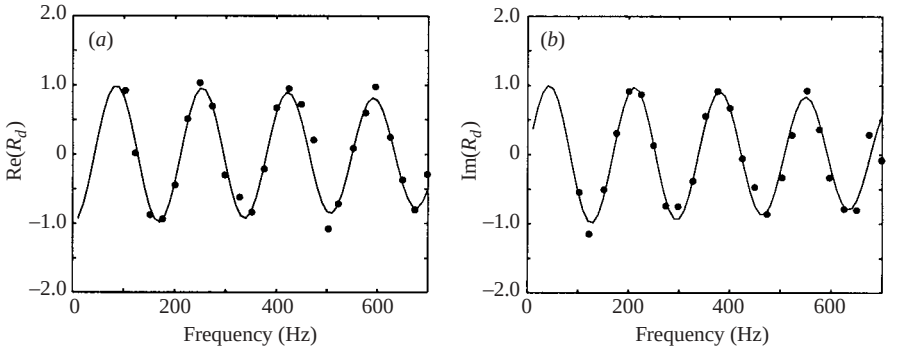

FIGURE 3. (*a*) Real and (*b*) imaginary parts of the downstream reflection coefficient for $M_{h,1} = 0.023$ and $M_u = 0$. Experiment: ●; model: ——.

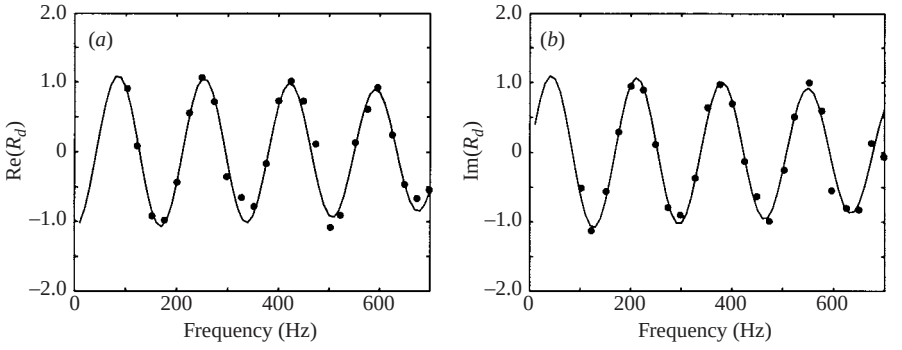

FIGURE 4. (*a*) Real and (*b*) imaginary parts of downstream reflection coefficient for $M_{h,1} = 0.03$ and $M_u = 0.046$. Experiment: ●; model: ——.

as little as 10% at the minima. The similarity of the experimental results at the two different sound levels confirms that linear absorption mechanisms are dominant. The model predicts the absorption very well, though there is some disagreement above $kL \approx 1.75$. The measurements at higher frequencies are more prone to experimental error; the discrepancy at the largest value of kL (corresponding to 700 Hz) is probably due to such error, as the relative transducer calibration exhibited a large phase shift near this frequency. The disagreement at the trough of $kL \approx 1.8$ can be reasonably attributed to high sensitivity to the degree of interference between the left- and right-travelling waves in the liner. At this frequency, as will be explained below, a pressure minimum occurs at some position in the lined section. The total absorption across the liner is crucially dependent on the magnitude of the pressure near this minimum. If this magnitude is over-predicted by the model, then the absorption trough will be shallower, as is seen in figure 5.

The results from a larger mean bias flow, $M_{h,1} = 0.041$, no mean duct flow, and sound pressure level at 100 dB are depicted in figure 6. The same oscillatory behaviour is evident, but the peak absorption values are only around 70% now; the minimum values are comparable to the previous case, however. At lower frequencies the agreement of the model with measured values is excellent, but the comparison is less favourable above $kL \approx 1.7$. The experimentally observed absorption is generally lower in the upper range of frequencies, and only rises to 55% at the final peak, instead of the 60% predicted by the model.

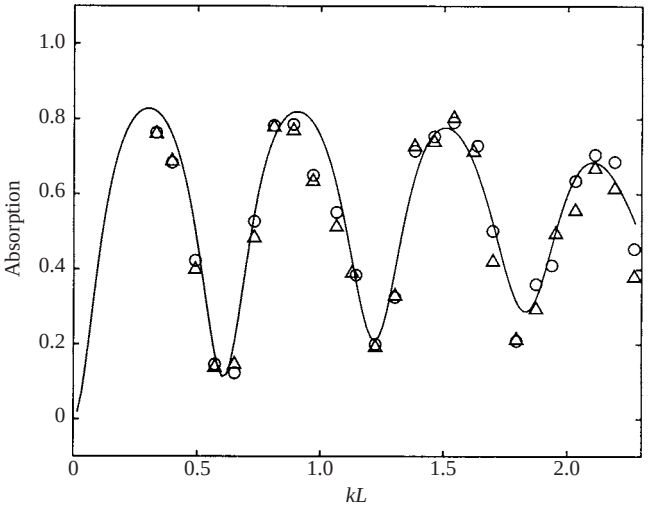

FIGURE 5. Absorption with varying frequency for $M_{h,1} = 0.023$ and $M_u = 0$. Experiment, 100 dB: ○; experiment, 115 dB: △; model: ——.

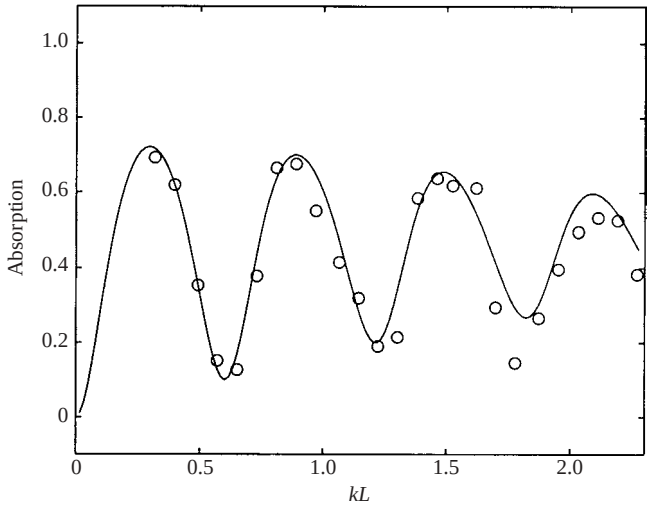

FIGURE 6. Absorption with varying frequency for $M_{h,1} = 0.041$ and $M_u = 0$. Experiment, 100 dB: ○; model: ——.

We now assess the effect of a small mean duct flow on the absorption. In figure 7 are depicted the results of experiments conducted with a mean duct flow of $M_u = 0.046$ and liner bias flow of $M_{h,1} = 0.030$, and at two different sound pressure levels, 100 dB and 115 dB. The character of the absorption is very similar to that of the previous cases, with peaks at nearly 80%. As in the first case, no significant variations are observed in the results from the two different sound pressure levels, so nonlinear absorption mechanisms are again negligibly small. The model once again predicts the absorption very well.

In the final case of this type we consider a slightly larger mean duct flow, $M_u = 0.057$, and a smaller mean bias flow, $M_{h,1} = 0.009$, with a sound pressure level of 100 dB. Figure 8 depicts the results. Though the experimental results exhibit behaviour

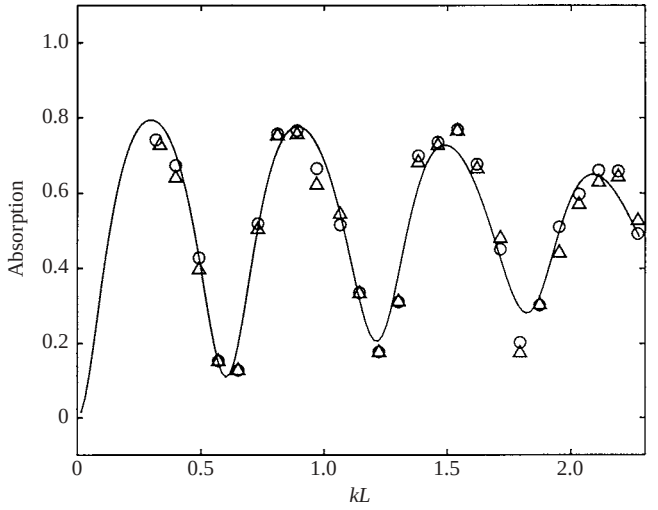

FIGURE 7. Absorption with varying frequency for $M_{h,1} = 0.030$ and $M_u = 0.046$. Experiment, 100 dB: ○; experiment, 115 dB: △; model: ——.

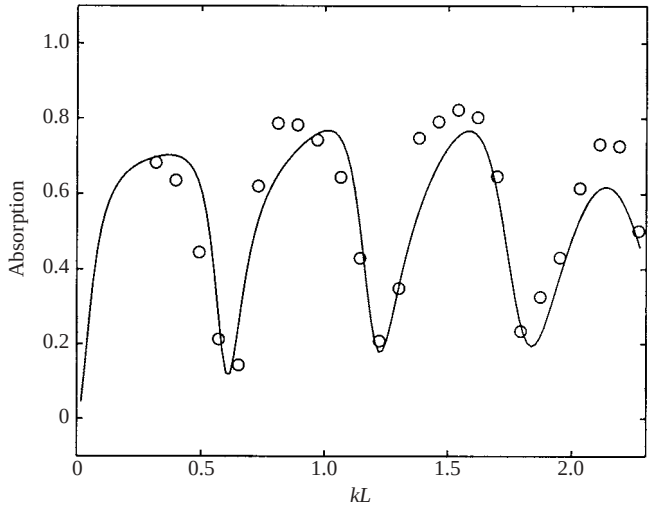

FIGURE 8. Absorption with varying frequency for $M_{h,1} = 0.009$ and $M_u = 0.057$. Experiment, 100 dB: ○; model: ——.

similar to the previous cases, the model predicts absorption peaks that are more rounded than in previous cases. Consequently, the agreement is poor near these peaks, though it is satisfactory at the absorption minima.

The four sets of experiments described were all conducted with constant flow conditions and varying frequency. They demonstrated that the model performs very well in predicting the absorption over a range of frequencies. Now we present the results when the frequency is held fixed and the mean liner bias flow varied. No mean duct flow is present and the sound pressure level is constant at 100 dB. The absorption at four different frequencies is depicted in figure 9. Frequencies of $kL = 0.89$, 1.54 and 2.11 correspond to absorption peaks in the previous cases, and $kL = 1.22$ corresponds to a minimum. In the absorption peak cases, the absorption reaches a maximum at

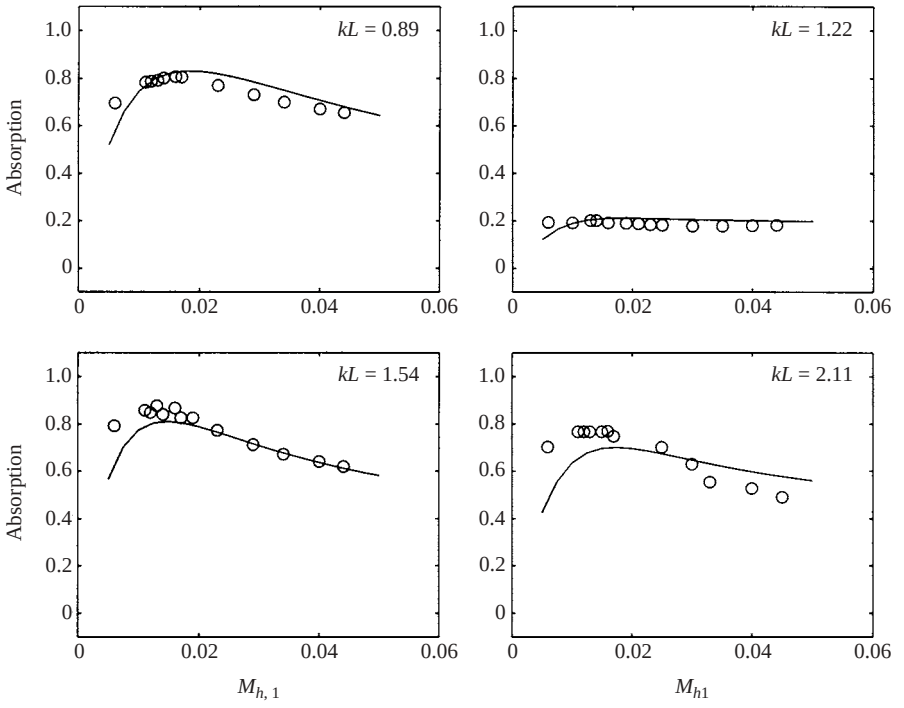

FIGURE 9. Absorption with varying mean bias flow and $M_u = 0$. Experiment, 100 dB: ○; model: ——.

around 82% at approximately the same flow, $M_{h,1} \approx 0.015$, and decays gradually as the flow is increased. The model predicts this behaviour well at low frequencies, but performs poorly at the highest frequency, $kL = 2.11$. At $kL = 1.22$, both experiment and model agree at a nearly constant value of around 20%.

5. Liner system design

5.1. *Maximizing absorption*

From a design standpoint, it is desirable to find the geometric and flow parameters for maximum absorption. Such an optimization problem is complicated by the number of parameters involved. For example, for a single liner in Configuration 1, the geometric parameters that appear in the model equations are (dropping the '1' subscript for brevity): the open-area ratio, σ; the scaled aperture radius, a/L; the scaled liner thickness, t/L; and the duct geometric parameter, CL/S_p. The flow parameters are: the scaled frequency, kL; the aperture Mach number, M_h; and the duct Mach number, M_u. Furthermore, we will show that the absorption is intimately connected to (and potentially enhanced by) the downstream configuration, so the design process should incorporate R_d. An additional liner increases the complexity still further. We will approach the design process systematically, beginning by identifying our goals and then reducing the problem to its barest essentials in a single, infinitesimally thin liner. Only then will we include a second liner in the design, developing an expression that describes the sharing of absorption between the two liners.

The absorption expression (4.3) provides a useful starting point. Provided the magnitude of the downstream reflection is less than or equal to unity, as is normally

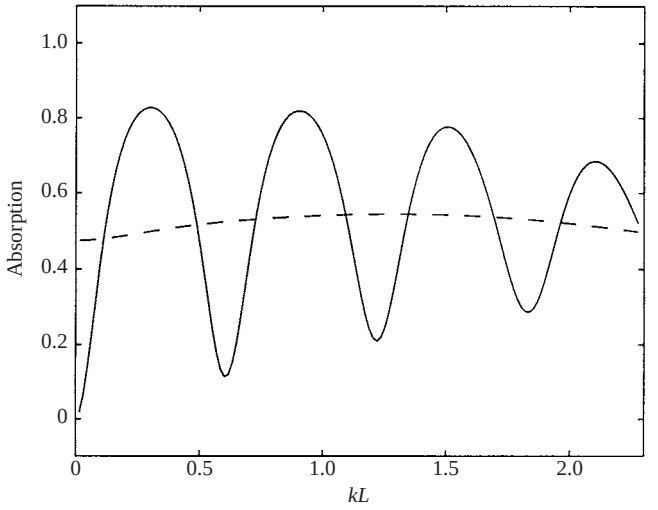

FIGURE 10. Comparison of absorption in a duct with $M_{h,1} = 0.023$ and $M_u = 0$, and with downstream length $L_d/L = 4.5$: ——; $L_d/L = \infty$: — — —.

true, this expression confirms what is intuitively obvious, that absorption is large when the acoustic energy transmitted, $|\psi^+(1)|^2$, and reflected, $|\psi^-(0)|^2$, by the liner system are both small. Because the downstream reflection may not be as simple as an open end, one approach would be to assume nothing about the downstream configuration and optimize the liner system in a duct that extends to infinity downstream (i.e. $R_d = 0$). This approach will lead to adequate results, but does not exploit the potential enhancement that arises from most practical downstream arrangements. For example, figure 10 depicts the absorption of a liner system in both semi-infinite and finite duct configurations. The absorption is substantially increased in certain frequency bands. It is important to incorporate such enhancement into the design process directly. Consequently, we will assume that the downstream configuration allows most of the acoustic energy to reflect back towards the liner (i.e. $|R_d| \approx 1$), and optimize the liner arrangement such that the resulting absorption peaks are as large as possible.

Because small transmission and reflection coincide with large absorption, it is natural to enquire whether the minima of these two quantities naturally coincide, and if not, whether we can force them to. In the Appendix, the single-liner equations are solved in the absence of mean duct flow, and the solution related to the semi-infinite downstream duct result. Relations (A 7*a*, *b*) for the transmitted and reflected energies immediately exhibit some essential features of the finite-duct results. In particular, the transmitted wave energy, equation (A 7*a*), can be enhanced or diminished depending only on the phase of the product $\tilde{R}_d \psi_\infty^-(0)$. The smallest transmission will occur when this phase is an odd multiple of π,

$$\arg(\tilde{R}_d \psi_\infty^-(0)) = (2n - 1)\pi. \tag{5.1}$$

Furthermore, larger magnitude of $\psi_\infty^-(0)$ will lead to greater deviation of this transmitted wave from its semi-infinite result.

Insight into the reflected wave amplitude is not as easy to obtain: relation (A 7*b*) demonstrates that the reflected energy is dependent upon a strong coupling between the left- and right-going waves in the liner. The phases of $\tilde{R}_d \psi_\infty^-(0)$

and $\tilde{R}_d\psi_\infty^{-*}(0)[(\psi_\infty^-(0))^2-(\psi_\infty^+(1))^2]$ appear in the denominator and numerator, respectively. With some rearrangement to isolate $\tilde{R}_d$, though, the phases can be regrouped into the phases of $\tilde{R}_d\psi_\infty^-(0)$ and $1-(\psi_\infty^+(1)/\psi_\infty^-(0))^2$. Thus, minimum reflection is not simply determined by equation (5.1), but by an intractable expression involving both phases. In general, these phases are uncorrelated, and therefore the reflection and transmission minima do not necessarily coincide. Furthermore, because of the complicated dependence of the semi-infinite solution on frequency, it proves impractical to tailor the liner so that they do coincide. However, we shall show that the minima do approximately coincide at low frequency, gradually diverging as frequency increases.

In fact, relying on the full frequency-dependent solution for optimization is impractical in many respects, so we instead follow a simpler approach. The long-wavelength limit $kL\to 0$ of the semi-infinite duct solution, though not interesting in itself, provides at least a reasonable prediction of the behaviour at low frequency, particularly because this solution tends to vary more slowly with frequency than $\tilde{R}_d$. We will therefore substitute the limiting values of $\psi_\infty^+(1)$ and $\psi_\infty^-(0)$ into the finite-duct relations (A 7a, b), and optimize the resulting approximate absorption.

With η given by equation (2.29) and $t/L=0$, the liner compliance factor $\eta/(\mathrm{i}kL)$ remains non-zero as kL approaches zero:

$$\lim_{kL\to 0}\frac{\eta}{\mathrm{i}kL}=\frac{1}{2}\frac{\sigma}{M_h}. \tag{5.2}$$

This limit can be interpreted in terms of a loss of dynamic head. A steady jet emerges from each aperture, in which the steady perturbation of the pressure is related to the velocity perturbation by $p_j'=-M_j v_j'$ through a non-dimensional version of Bernoulli's theorem. If this jet loses all of its dynamic head as it empties into the duct and dissipates, then the stagnation pressure (or enthalpy) in the duct will be equal to its static value in the jet, $B'\approx p_j'$. The velocity perturbation of the jet is related to the liner velocity through $v_j'=v'/\sigma$. Howe (1979b) argues that the mean jet velocity is twice the mean aperture velocity because of the vena contracta. Thus, we find that $v'/B'\approx -\sigma/(2M_h)$, which is simply the negative of $\eta/(\mathrm{i}kL)$.

The liner equations in the limit of long-wavelength reduce to

$$\frac{\mathrm{d}\psi^+}{\mathrm{d}x}=-b(\psi^++\psi^-), \tag{5.3a}$$

$$\frac{\mathrm{d}\psi^-}{\mathrm{d}x}=b(\psi^++\psi^-), \tag{5.3b}$$

where

$$b\equiv\frac{CL}{4S_p}\frac{\sigma}{M_h}. \tag{5.4}$$

A steady perturbation to the stagnation enthalpy maintains a steady and uniform difference across the liner, which therefore draws a liner flow that causes the velocity perturbation to vary linearly along the length of the liner. The semi-infinite duct transmission and reflection are thus, respectively,

$$\psi_\infty^+(1)=\frac{1}{1+b},\quad \psi_\infty^-(0)=-\frac{b}{1+b}. \tag{5.5}$$

Substituting these into the finite-duct expressions, and assuming that $|\tilde{R}_d| = 1$, then

$$|\psi^+(1)|^2 = \frac{1}{(1+b)^2 + b^2 - 2b(1+b)\cos\phi_R}, \tag{5.6a}$$

$$|\psi^-(0)|^2 = \frac{(1-b)^2 + b^2 + 2b(1-b)\cos\phi_R}{(1+b)^2 + b^2 - 2b(1+b)\cos\phi_R}, \tag{5.6b}$$

where $\phi_R \equiv \arg(-\tilde{R}_d) = \arg(-R_d) + 2kL$ is a long-wavelength approximation of $\arg(\tilde{R}_d \psi_\infty^-(0))$. The limiting phase of $1 - (\psi_\infty^+(1)/\psi_\infty^-(0))^2$ is either π (when $b < 1$) or 0 (when $b > 1$), though both ensure that the minima of reflection and transmission coincide, which, as equation (5.1) predicts, will occur when $\phi_R = (2n-1)\pi$, where n is some integer. At these minima the transmitted and reflected energies are determined by b. At $b = 0$, the liner is effectively rigid and thus both energies are equal to the incident energy (since the reflection is perfect). Increasing b causes both the transmitted and reflected energies to decrease steadily until $b = 1/2$, at which the reflected energy is zero but the transmitted energy is still finite. Beyond $b = 1/2$, the transmitted energy continues to decay, approaching zero as $b \to \infty$, but the amount of reflected energy increases. Note that, because the transmitted energy never reaches zero, the liner system can never absorb *all* incident acoustic energy.

Substituting (5.6*a*, *b*) into the absorption expression (4.3), we arrive at

$$\Delta = \frac{2b(1-\cos\phi_R)}{1 + b(b+1)(1-\cos\phi_R)}. \tag{5.7}$$

As expected, the absorption maxima occur at the coincident minima of reflection and transmission, at $\phi_R = (2n-1)\pi$. The value of b that gives the greatest absorption at these maxima is $1/\sqrt{2}$, at which $\Delta = 0.8284$. Therefore, for a single liner configuration, the liner parameters should as closely as possible obey

$$\left(\frac{M_h}{\sigma}\right)_{opt} = \frac{CL/S_p}{2\sqrt{2}}. \tag{5.8}$$

This optimum relation will become less valid at higher frequency, particularly if $\tilde{R}_d$ does not vary significantly faster with kL than the semi-infinite duct results (for instance, when $L_d/L \lesssim 1$). But it should at least provide a reasonable guideline for choosing parameters. Note that the ratio of hole diameter to liner length, a/L, does not appear in this expression.

When there are two liners, the absorption load is shared by both liners. Again, we make the assumption that the semi-infinite downstream duct solution varies more slowly with frequency than $\tilde{R}_d$. Because of the relationships between the geometric and flow parameters, it can be verified that the differential equation for the acoustic velocity between the liners (equation (2.21*b*)) reduces to

$$\frac{\mathrm{d}u_1}{\mathrm{d}x} = -2b\frac{(C_1/C_2)^2}{1-(C_1/C_2)^2}\left\{\left[1 + \left(\frac{C_2}{C_1}\right)^2\left(\frac{\sigma_2}{\sigma_1}\right)^2\right]\hat{B}_1 - \psi^+ - \psi^-\right\}, \tag{5.9}$$

where b is defined as before. The stagnation enthalpy fluctuations both in the duct and between the liners are uniform, and thus the solution of (5.9) must vary linearly. However, to satisfy the no-throughflow conditions at both ends of the liner, there can be no variation and the term in curly brackets in (5.9) must vanish. Thus the

stagnation enthalpy fluctuations on either side of the inner liner are related by

$$\left[1+\left(\frac{C_2}{C_1}\right)^2\left(\frac{\sigma_2}{\sigma_1}\right)^2\right]\hat{B}_1=\psi^+ +\psi^-=\hat{B}. \tag{5.10}$$

Substituting this into the corresponding duct equations, we arrive at

$$\frac{\mathrm{d}\psi^+}{\mathrm{d}x}=-\frac{b}{(\sigma_1/\sigma_2)^2(C_1/C_2)^2+1}(\psi^+ +\psi^-), \tag{5.11a}$$

$$\frac{\mathrm{d}\psi^-}{\mathrm{d}x}=\frac{b}{(\sigma_1/\sigma_2)^2(C_1/C_2)^2+1}(\psi^+ +\psi^-). \tag{5.11b}$$

Comparing these with (5.3*a*, *b*) reveals that we need only modify our definition of the parameter b when a second liner is included, and thus the optimal value of $M_{h,1}/\sigma_1$ is now

$$\left(\frac{M_{h,1}}{\sigma_1}\right)_{opt}=\frac{(M_h/\sigma)_{opt,sl}}{(\sigma_1/\sigma_2)^2(C_1/C_2)^2+1}, \tag{5.12}$$

where $(M_h/\sigma)_{opt,sl}$ is the single-liner result given by (5.8). For small σ_1/σ_2, the inner liner is absorbing the larger fraction of energy. As σ_1/σ_2 grows the absorption load is transferred to the outer liner, and when $\sigma_1/\sigma_2=C_2/C_1$, the liners share the load equally. Note that, because $C_2/C_1>1$, identical inner and outer liners do not absorb equally.

Note that expression (5.12) does not provide guidance on how to choose the ratios C_1/C_2 or σ_1/σ_2. Our simple long-wavelength approach only states that, provided the parameters are chosen to satisfy (5.12), the absorption peaks of the liner system will be approximately 83%. Solution of the full model reveals that certain choices of these ratios do lead to marginally better absorption, but the improvement is too slight to be incorporated into the design process.

It is useful to check these expressions with the experimental results of §4. For the liner system used, $C_1L/S_p=5.58$, $C_2/C_1=1.20$, $\sigma_1=0.040$ and $\sigma_2=0.020$. Thus, equation (5.8) predicts $(M_h/\sigma)_{opt,sl}=1.97$ and relation (5.12) produces $(M_{h,1}/\sigma_1)_{opt}=0.52$. The optimal aperture Mach number, $M_{h,1}=0.021$, compares favourably with the observed peak in the experimental results of figure 9, which occurs at $M_{h,1}\approx 0.015$ for the three peak frequencies. Furthermore, the predicted absorption of 83% is very close to the observed values at the peaks in figure 9.

5.2. *Positions of absorption extrema*

In the previous section we used the argument that the long-wavelength limit of the semi-infinite duct solution could be used for deriving the optimal parameters. We now explore whether the same limit can be used to predict the positions of absorption extrema.

Expressions (5.6*a*, *b*) indicate that the minima and maxima of the finite-duct reflection coincide with those of the transmission at low frequency, at values of kL determined by $\phi_R=(2n-1)\pi$ and $\phi_R=2n\pi$, respectively. Consequently, the absorption maxima are quite strong at low frequency, as indeed are the absorption minima. Our approximate expression for the absorption predicts that it will vanish entirely at the minima. Though this is not true in practice, the minimum values observed in the experimental results of §4 are indeed quite small.

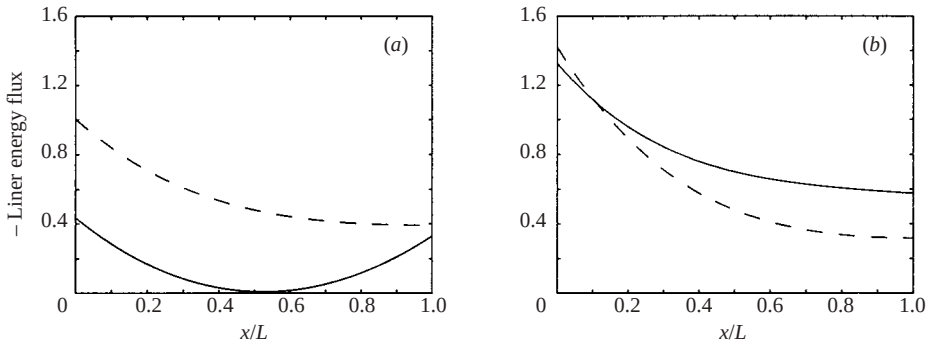

FIGURE 11. Acoustic energy flux through the liner for a single-liner system at $M_{h,1} = 0.04$ at (*a*) $kL = 0.60$ and (*b*) $kL = 0.98$. $L_d/L = 4.5$: ——; $L_d/L = \infty$: — — —.

However, whilst the long-wavelength limit successfully predicts the value of maximum absorption at finite frequencies when the parameters are optimal (as comparison with figure 9 demonstrated), the values of kL at which the absorption extrema occur are poorly predicted by $\phi_R = (2n-1)\pi$ and $\phi_R = 2n\pi$. As frequency increases, the phases of the semi-infinite transmission and reflection amplitudes both drift from their long-wavelength values. Consequently, the phase of $\tilde{R}_d \psi_\infty^-(0)$ deviates from ϕ_R, and the peaks and troughs of transmission and reflection tend to separate. Instead of relying on the same limiting approach for predicting the frequencies of absorption extrema, we will develop semi-empirical relations.

The acoustic energy flux through the liner provides insight into the absorption minima. Figure 11(*a*) depicts (the negative of) the liner energy flux for a single-liner system with mean bias flow $M_{h,1} = 0.040$ at $kL = 0.60$, which corresponds to an absorption minimum. The results for both finite (open-ended) and semi-infinite downstream ducts are shown. The plot reveals that for the finite-length case, the energy flux through the liner is negligibly small at a position approximately 54% of the liner length. The total absorption, which corresponds to the area under the liner flux curve, is consequently small.

A node in the stagnation enthalpy at this position of minimum flux prevents energy from travelling through the liner. The presence of the node is made possible by the downstream reflection, which leads to a standing wave supported by the downstream section as well as a latter portion of the lined section. In fact, the frequencies of minimum absorption can be predicted approximately by using this standing-wave argument. For certain ranges of frequencies, the standing wave will have a node in the lined section. The node is not complete because liner absorption prevents total interference, and it becomes weaker as it moves toward the upstream end of the section. Minimum absorption occurs when the influence of this node has the greatest axial extent, which occurs when the node is located at some fractional distance ϕ from the downstream end of the lined section. For example, in figure 11(*a*), $\phi \approx 0.46$. Since the open duct ensures a node at the duct exit, frequencies at which multiples of half-wavelengths are supported in the section of scaled length $L_d/L + \phi + \delta/L$, where δ/L is a correction length to account for absorption, approximately coincide with absorption minima, predicted by

$$(kL)_{min}^{(n)} = \frac{n\pi}{L_d/L + \phi_{min} + \delta_{min}/L}. \tag{5.13}$$

From an analysis of results for several values of L_d/L and $M_{h,1}$, in both single- and double-liner systems, we have found that when

$$\phi_{min} \approx 0.46, \quad \delta_{min}/L \approx 0.05, \tag{5.14}$$

the frequencies are predicted well by (5.13).

The standing-wave argument does not apply as neatly to predicting absorption maxima. The liner energy flux does not attain a relative maximum in the lined section at maximum absorption as it does a relative minimum for minimum absorption. Rather, as figure 11(*b*) shows, the energy flux is maximum at the liner entrance and decays steadily with distance as energy is absorbed. Thus, it is difficult to argue for odd multiples of quarter-waves in some duct length coinciding with absorption maxima. However, the results for several sets of parameters can be reduced to a similar relation to (5.13), again for an open-ended duct,

$$(kL)^{(n)}_{max} = \frac{(n-1/2)\pi}{L_d/L + \phi_{max} + \delta_{max}/L}, \tag{5.15}$$

where, maintaining the same correction length as above,

$$\phi_{max} \approx 0.60, \quad \delta_{max}/L \approx 0.05. \tag{5.16}$$

It is important to note that the form assumed for the extrema positions will not hold in all circumstances. When the downstream duct is longer than the liner, the approach predicts the positions well. However, as L_d approaches L or becomes smaller, the formulae become increasingly sensitive to ϕ and δ/L, which must ultimately include their own frequency dependences.

5.3. *Alternative definition of absorption*

Equation (3.8) is not the only definition of absorption, and in some cases there are other definitions more appropriate for assessing the performance of an absorbing device. An absorption system is often used to prevent acoustic waves in a duct from returning to their source, and thus mitigate the growth of acoustically driven instabilities. The acoustic energy that is transmitted downstream of the liner section is inconsequential, particularly for a downstream section in which the bulk of this transmitted energy is reflected by the exit. In these circumstances, when $|R_d| \approx 1$, equation (3.8) reduces to

$$\Delta \approx \frac{|B_u^+|^2 - |B_u^-|^2}{|B_u^+|^2 + |B_d^+|^2}. \tag{5.17}$$

An alternative definition for the absorption is

$$\Delta_R \equiv 1 - \frac{|B_u^-|^2}{|B_u^+|^2}, \tag{5.18}$$

which is effectively a renormalization of the traditional absorption of (5.17). This new definition represents the deficit in the energy reflected upstream. For example, for an open-ended duct in the absence of any absorption system, nearly all energy travelling away from the source is reflected back toward it, and $\Delta_R \approx 0$. In contrast, a value of 1 for Δ_R would indicate that all outgoing energy is either absorbed or transmitted.

Figure 12 compares the two definitions of absorption using the model results in a two-liner system for the case of $M_{h,1} = 0.023$ and $M_u = 0$. The corresponding experimentally measured values of Δ_R are included, as well. Both absorption definitions oscillate with frequency, with extrema at the same frequencies. The absorption peaks

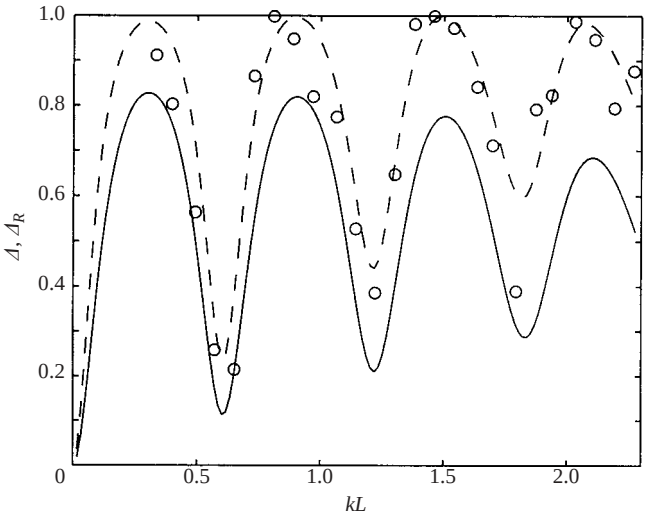

FIGURE 12. Comparison of absorption definitions for a double-liner system with $M_{h,1} = 0.023$ and $M_u = 0$. Δ, model: ——; Δ_R, model: — — —; Δ_R, experiment: ○.

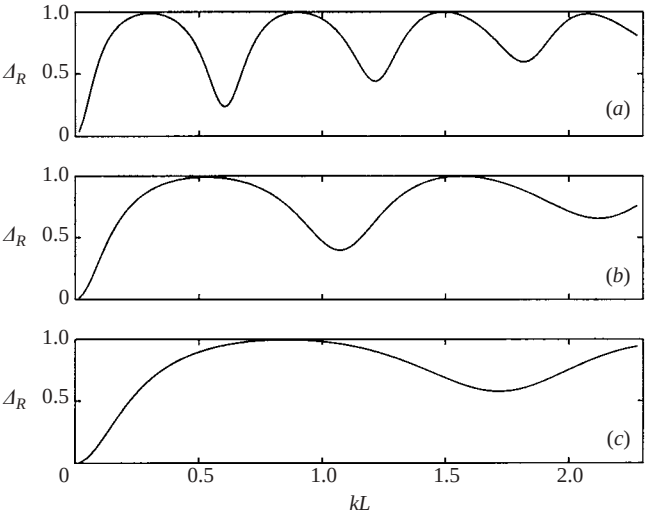

FIGURE 13. Evaluation of liner performance when varying L_d/L with $M_{h,1} = 0.023$ and $M_u = 0$. (*a*) $L_d/L = 4.5$, (*b*) $L_d/L = 2.25$, and (*c*) $L_d/L = 1.13$.

of Δ_R rise to 100%, however. Moreover, the absorption troughs are higher and become much shallower with increasing frequency (the low experimental value at $kL \approx 1.8$ was attributed in § 4.2 to a sensitive dependence on left/right wave cancellation).

This liner design is an example of an effective absorption system, but only very near the discrete frequencies of peak absorption. It is often the case that the frequencies of acoustic waves that should be suppressed are not known *a priori*, and thus it is undesirable for an absorption system to have such narrow bandwidths of effectiveness. We can use the analysis of § 5.2 to improve the design by spreading the absorption minima apart. Equation (5.13) suggests that this can be accomplished by decreasing the downstream duct length, L_d/L. In figure 13 the effect of varying L_d/L

is demonstrated. As L_d/L is first halved and then quartered, the absorption troughs are more separated and made more shallow. Furthermore, the absorption peaks are widened and maintained at 100%.

The extrema formulae, (5.13) and (5.15), can also be used effectively for predicting the minima and maxima of the alternative absorption, provided that kL is sufficiently small so that the reflection and transmission extrema are close, as discussed in § 5.2. It is useful to validate the formulae with the model results of figure 13. For $L_d/L = 4.5$, the minima are predicted to lie at $kL = 0.63$, 1.25 and 1.88, and the maxima at $kL = 0.31$, 0.92, and 1.53. These values are all near the observed values, though they tend to slightly overshoot the larger frequencies. At $L_d/L = 2.25$, the predicted minimum at $kL = 1.14$ and maxima at $kL = 0.54$ and 1.62 agree reasonably well, but with more overshoot at smaller kL than in the previous case. Finally, at $L_d/L = 1.13$, the first maximum appears near its expected position at $kL = 0.88$, but the first minimum occurs at a significantly smaller frequency than the predicted position of $kL = 1.92$. The usefulness of the formulae is limited at this small L_d/L.

6. Conclusions

In this work we have investigated the effectiveness of a perforated liner system with mean bias flow in the absorption of planar acoustic waves in a circular duct. The lined section of duct is composed of a homogeneous array of circular apertures, surrounded by a radially external region of larger mean pressure that forces a steady flow through each aperture. Planar sound waves produced by an upstream source travel through the lined section, subjecting each aperture to a harmonic pressure difference that causes the periodic shedding of vorticity from the aperture rim. The mechanism for absorption lies in this one-way transfer of acoustic energy into vortical energy, which is subsequently dissipated. Moreover, the fraction of incident acoustic energy that is absorbed is independent of the magnitude of the pressure difference. This linear mechanism is embodied in the aperture Rayleigh conductivity derived by Howe (1979*b*). In this work, we have developed a one-dimensional duct model with a homogeneous liner compliance based on this Rayleigh conductivity. The model is capable of describing both single- and double-liner configurations.

The comparison of this model with our experimental results demonstrates excellent agreement for a large range of frequencies and mean flow conditions. We have shown that such a system, when included in a duct whose termination allows most acoustic energy to reflect upstream for further interaction with the liner, can absorb as much as 83% of incident energy at certain frequencies, and prevent 100% of the outgoing energy from reflecting back to the source. Our analysis of the acoustic energy flux has revealed the local absorptive character of the liner. In particular, it has demonstrated that both liners in a double-liner system are important for absorption. Also, we have shown that the absorption troughs that occur at frequencies between the peaks are due to pressure nodes in the liner that limit the local absorption. The effect of these nodes is crucially dependent on the length of the downstream duct. As this length is shortened, the absorption troughs separate with respect to frequency and the absorption peaks consequently become broader.

Further insight has been gained by reducing the model equations through a long-wavelength limit $kL \to 0$ that identified the parameter $b = \frac{1}{4}(CL/4S_p)(\sigma/M_h)$ as particularly important in determining the effectiveness of the liner system as an absorber. As we have shown, these reduced equations contain an absorption term that can be interpreted as a loss in dynamic head of the steady jets issuing from

each aperture in the liner. Provided that the flow conditions and geometry of a single liner are designed so that $b \approx 1/\sqrt{2}$, the absorption peaks will be nearly maximal. Furthermore, we have shown that a double-liner configuration is equally effective when designed using a modified expression for b that accounts for the absorption load shared by each liner.

The mechanism for absorption implicit in the model is the same as that included in the reflection coefficient of Hughes & Dowling (1990), who also adapted the Rayleigh conductivity of Howe (1979*b*). The absorption of impinging acoustic waves considered by Hughes & Dowling (1990) depends on proximity to a Helmholtz resonance condition, involving the imaginary cavity behind each aperture. Absorption in the present model, however, is identified with the cumulative effect of local absorption over a duct section of finite length. The present work involves combining these two approaches to predict the absorption of both axial and radial acoustic modes.

It should be noted that, though we have only considered planar duct modes in this work, the liner system will also absorb circumferential modes by the same mechanism. A similar analysis is currently being undertaken to quantify its effectiveness in this respect. Also, the model equations can be adapted to incorporate combustion by allowing a mean temperature difference across the inner liner. Hughes & Dowling (1990) included an analysis that assumed that, in the presence of high combustion temperatures, the mean bias flow creates a thin layer adjacent to the liner with 'cold' properties. In the present case, acoustic waves only travel parallel to this layer rather than impinging upon it, so the effect of combustion would be limited to modifying the speed of sound and mean density in the duct.

This work was supported by the PRECCINSTA project, Contract No. ENK5-CT2000-00099, which was sponsored by the Fifth European Community Framework Programme. The authors are indebted to Dr Iain Dupère for many useful discussions. We would also like to thank Mr Dave Martin for building the experimental apparatus.

Appendix. Analytical solution of single-liner equations

In this Appendix we solve the liner equations (2.14*a*, *b*) for the special case of a single liner exposed to the ambient environment (Configuration 1). We will assume that there is no mean upstream duct flow, $\bar{u}_u = 0$, and that the liner bias flow is sufficiently small that $\bar{u}_d \approx 0$. Thus, the liner equations reduce to the system

$$\frac{\mathrm{d}\psi^+}{\mathrm{d}x} = -\left(\mathrm{i}kL + \frac{\Gamma}{2}\frac{\eta}{\mathrm{i}kL}\right)\psi^+ - \frac{\Gamma}{2}\frac{\eta}{\mathrm{i}kL}\psi^-, \tag{A 1a}$$

$$\frac{\mathrm{d}\psi^-}{\mathrm{d}x} = \left(\mathrm{i}kL + \frac{\Gamma}{2}\frac{\eta}{\mathrm{i}kL}\right)\psi^- + \frac{\Gamma}{2}\frac{\eta}{\mathrm{i}kL}\psi^+, \tag{A 1b}$$

where $\Gamma \equiv CL/S_p$, and the numerical liner subscript has been removed for brevity. The boundary conditions are

$$\psi^+(0) = 1, \tag{A 2a}$$

$$\psi^-(1) - \tilde{R}_d\psi^+(1) = 0. \tag{A 2b}$$

The factor $\tilde{R}_d$ is a modified reflection coefficient, related to the previously defined coefficient by $\tilde{R}_d = R_d \exp(\mathrm{i}2kL)$. We have assumed that all acoustic quantities are scaled by the incident wave amplitude, B_u^+.

The eigenvalues of this system of two first-order linear equations are given by

$$\lambda = \pm(-k^2L^2 + \Gamma\eta)^{1/2}. \tag{A 3}$$

The expression under the square root is complex and to avoid messy formulae the eigenvalues are left unevaluated. The solution of the system is

$$\psi^+(x) = \frac{[(\lambda^2 - k^2L^2) + \tilde{R}_d(\lambda^2 + k^2L^2)]\sinh\lambda(1-x) + \mathrm{i}2kL\lambda\cosh\lambda(1-x)}{[(\lambda^2 - k^2L^2) + \tilde{R}_d(\lambda^2 + k^2L^2)]\sinh\lambda + \mathrm{i}2kL\lambda\cosh\lambda}, \tag{A 4a}$$

$$\psi^-(x) = \frac{[(\lambda^2 + k^2L^2) + \tilde{R}_d(\lambda^2 - k^2L^2)]\sinh\lambda(1-x) - \mathrm{i}2kL\lambda\tilde{R}_d\cosh\lambda(1-x)}{[(\lambda^2 - k^2L^2) + \tilde{R}_d(\lambda^2 + k^2L^2)]\sinh\lambda + \mathrm{i}2kL\lambda\cosh\lambda}. \tag{A 4b}$$

Equations (A 4*a*, *b*) do not readily provide understanding of the physics in the lined section. However, it is useful to relate this solution, for which the reflection coefficient is general, to the solution for $\tilde{R}_d = 0$, which corresponds to a semi-infinite downstream section. With some manipulation, it can be shown that

$$\psi^+_\infty(0)\psi^+(x) = \psi^+(0)\psi^+_\infty(x) + \psi^-(1)\psi^-_\infty(1-x), \tag{A 5a}$$

$$\psi^+_\infty(0)\psi^-(x) = \psi^+(0)\psi^-_\infty(x) + \psi^-(1)\psi^+_\infty(1-x), \tag{A 5b}$$

where the subscript ∞ denotes the semi-infinite duct solution. Though the physical significance of these relations is limited, they provide useful expressions when evaluated at the ends of the lined section. When the first is evaluated at $x = 1$ and the second at $x = 0$, the wave amplitudes of both solutions in the upstream and downstream ducts are related:

$$\psi^+_\infty(0)\psi^+(1) = \psi^+(0)\psi^+_\infty(1) + \psi^-(1)\psi^-_\infty(0), \tag{A 6a}$$

$$\psi^+_\infty(0)\psi^-(0) = \psi^+(0)\psi^-_\infty(0) + \psi^-(1)\psi^+_\infty(1), \tag{A 6b}$$

providing, in effect, a transfer function from the incoming waves, $\psi^+(0)$ and $\psi^-(1)$, to the outgoing waves, $\psi^+(1)$ and $\psi^-(0)$. An obvious application of this transfer function is for transforming results for a duct of general end condition into results for a semi-infinite duct.

When we apply the boundary conditions on ψ^+ and ψ^- to relations (A 6*a*, *b*), rearrange, and take their absolute values, we arrive at

$$|\psi^+(1)|^2 = \left|\frac{\psi^+_\infty(1)}{1 - \tilde{R}_d\psi^-_\infty(0)}\right|^2, \tag{A 7a}$$

$$|\psi^-(0)|^2 = \left|\frac{\psi^-_\infty(0) - \tilde{R}_d[(\psi^-_\infty)^2(0) - (\psi^+_\infty)^2(1)]}{1 - \tilde{R}_d\psi^-_\infty(0)}\right|^2. \tag{A 7b}$$

REFERENCES

Bellucci, V., Paschereit, C. O. & Flohr, P. 2002 Impedance of perforated screens with bias flow. *AIAA Paper* 2002-2437.

Cargill, A. M. 1982*a* Low frequency acoustic radiation from a jet pipe – a second order theory. *J. Sound Vib.* **83**, 339–354.

Cargill, A. M. 1982*b* Low-frequency sound radiation and generation due to the interaction of unsteady flow with a jet pipe. *J. Fluid Mech.* **121**, 59–105.

Crighton, D. G. 1985 The Kutta condition in unsteady flow. *Annu. Rev. Fluid Mech.* **17**, 411–445.

Cummings, A. 1983 Acoustic nonlinearities and power losses at orifices. *AIAA J.* **22**, 786–792.

Dowling, A. P. & Hughes, I. J. 1992 Sound absorption by a screen with a regular array of slits. *J. Sound Vib.* **156**, 387–405.

Dupère, I. D. J. & Dowling, A. P. 2000 Absorption of sound near abrupt area expansions. *AIAA J.* **38**, 193–202.

Ffowcs Williams, J. E. 1972 The acoustics of turbulence near sound-absorbent liners. *J. Fluid Mech.* **51**, 737–749.

Follet, J. I., Betts, J. F. & Kelly, J. J. 2001 Improvements to acoustic liner broadband absorption using bias flow. *AIAA Paper* 2001-0823.

Howe, M. S. 1979*a* Attenuation of sound in a low Mach number nozzle flow. *J. Fluid Mech.* **91**, 209–229.

Howe, M. S. 1979*b* On the theory of unsteady high Reynolds number flow through a circular aperture. *Proc. R. Soc. Lond.* A **366**, 205–223.

Howe, M. S. 1986 Attenuation of sound due to vortex shedding from a splitter plate in a mean duct flow. *J. Sound Vib.* **105**, 385–396.

Howe, M. S., Scott, M. I. & Sipcic, S. R. 1996 The influence of tangential mean flow on the Rayleigh conductivity of an aperture. *Proc. R. Soc. Lond.* A **452**, 2303–2317.

Hughes, I. J. & Dowling, A. P. 1990 The absorption of sound by perforated linings. *J. Fluid Mech.* **218**, 299–335.

Jing, X. & Sun, X. 1999 Experimental investigations of perforated liners with bias flow. *J. Acoust. Soc. Am.* **106**, 2436–2441.

Jing, X. & Sun, X. 2000 Effect of plate thickness on impedance of perforated plates with bias flow. *AIAA J.* **38**, 1573–1578.

Ko, S.-H. 1972 Sound attenuation in acoustically lined circular ducts in the presence of uniform flow and shear flow. *J. Sound Vib.* **22**, 193–210.

Leppington, F. G. 1977 The effective compliance of perforated screens. *Mathematika* **24**, 199–215.

Leppington, F. G. & Levine, H. 1973 Reflexion and transmission at a plane screen with periodically arranged circular or elliptical apertures. *J. Fluid Mech.* **61**, 109–127.

Levine, H. & Schwinger, J. 1948 On the radiation of sound from an unflanged circular pipe. *Phys. Rev.* **73**, 383–406.

Morfey, C. L. 1971 Acoustic energy in non-uniform flows. *J. Sound Vib.* **14**, 159–170.

Munt, R. M. 1977 The interaction of sound with a subsonic jet issuing from a semi-infinite cylindrical pipe. *J. Fluid Mech.* **83**, 609–640.

Munt, R. M. 1990 Acoustic transmission properties of a jet pipe with subsonic jet flow. I. The cold jet reflection coefficient. *J. Sound Vib.* **142**, 413–436.

Peters, M. C. A. M., Hirschberg, A., Reijnen, A. J. & Wijnands, A. P. J. 1993 Damping and reflection coefficient measurements for an open pipe at low Mach and low Helmholtz numbers. *J. Fluid Mech.* **256**, 499–534.

Press, W. H., Teukolsky, S. A., Vetterling, W. T. & Flannery, B. P. 1986 *Numerical Recipes*. Cambridge University Press.

Rienstra, S. W. 1983 A small Strouhal number analysis for acoustic wave-jet flow-pipe interaction. *J. Sound Vib.* **86**, 539–556.

Sbardella, L., Tester, B. J. & Imregun, M. 2001 A time-domain method for the prediction of sound attenuation in lined ducts. *J. Sound Vib.* **239**, 379–396.

Seybert, A. F. & Ross, D. F. 1977 Experimental determination of acoustic properties using a two-microphone random-excitation technique. *J. Acoust. Soc. Am.* **61**, 1362–1370.

Seybert, A. F. & Soenarko, B. 1981 Error analysis of spectral estimates with application to the measurement of acoustic parameters using random sound fields in ducts. *J. Acoust. Soc. Am.* **69**, 1190–1199.

Tam, C. K. W., Kurbatskii, K. A., Ahuja, K. K. & Gaeta, Jr., R. J. 2001 A numerical and experimental investigation of the dissipation mechanisms of resonant acoustic liners. *J. Sound Vib.* **245**, 545–557.